Nonlinear resonance in the hydrogen atom

Marshall Burns* and L. E. Reichl
Center for Studies in Statistical Mechanics and Complex Systems, The University of Texas at Austin, Austin, Texas 78712
(Received 20 May 1991; revised manuscript received 8 July 1991)

The size and location of nonlinear-resonance zones, in the one-dimensional model microwave-driven hydrogen, are obtained numerically for the microwave field strengths and frequency used in experiments. Classical simulations show a high correlation between the widths of fractional resonances at the chaos border and the width of regions of suppressed ionization observed in experiments. Numerical evidence is given for the existence of quantum nonlinear resonances in microwave-driven hydrogen.

PACS number(s): 32.80.Rm, 03.65.Sq

I. INTRODUCTION

Since the mid-1970s, there has been a significant experimental effort to determine the behavior of highly excited states of hydrogen perturbed by electromagnetic microwaves [1–11]. The excited states are prepared by laser excitation in the presence of a static electric field. They are *extreme Stark* or *one-dimensional* states and are most conveniently described in terms of parabolic quantum numbers $(n;n_1,n_2,m)$ [12], where $n=n_1+n_2+|m|+1$ is the principal quantum number. The atoms entering the microwave cavity are typically in eigenstates $(n;0,n-1,0)$ or $(n;1,n-2,0)$ where $30<n<90$. In these states, the classical orbit or the quantum-mechanical orbital of the electron lies almost along a straight line and the electron remains predominantly on one side of the proton. The static electrostatic field is used to prepare the initial states, and may or may not be active in the region of the microwave perturbation. Because of this preparation of the atom the relative motion of the electron and proton in the presence of the microwave field is described fairly well in terms of a one-dimensional model,

$$H=\tfrac{1}{2}p^2-\frac{1}{x}+Fx\cos(\omega t)\ , \tag{1.1}$$

where p and x are the relative momentum and displacement of the electron and proton, respectively, and F and ω are the peak electric-field strength and angular frequency of the microwave field, respectively (in atomic units). As we shall show, this one-dimensional classical model (which we shall call the harmonically driven Stark states of hydrogen, or the HSH model) goes far in reproducing the observed behavior of hydrogen in the microwave field.

Koch and others [5,8] have measured the amplitude of the microwave field needed to ionize hydrogen for a range of principal quantum numbers. Their results are shown in Fig. 1. The overall downward trend reflects the fact that it takes less force to ionize a more highly excited atom. The reversal of the downward trend that occurs at $n=82$ marks the lower edge of the first primary resonance (we define primary resonances in Sec. II) and therefore the edge of the chaotic sea formed by the overlap of the primary and higher-order resonances. (A region in which primary and higher-order resonances have overlapped is one in which all Kolmogorov-Arnold-Moser (KAM) tori which might block the flow of trajectories to higher values of action, and ultimately to the continuum, have been destroyed.) There are regions below $n=82$ where the ionization threshold forms plateaus over a range of several energy levels. Jensen [13] has suggested that these plateaus or stable regions correspond to fractional resonance zones in the phase space of the hydrogen atom. But this has raised two questions that have gone unanswered until now.

(1) The centers of the stable regions in the space of energy levels match very closely the predicted locations of particular fractional resonance zones. But do the resonance zones also account for the *widths* of the stable regions? This question is answered here, in the affirmative, by numerical simulations of the behavior of the atom at

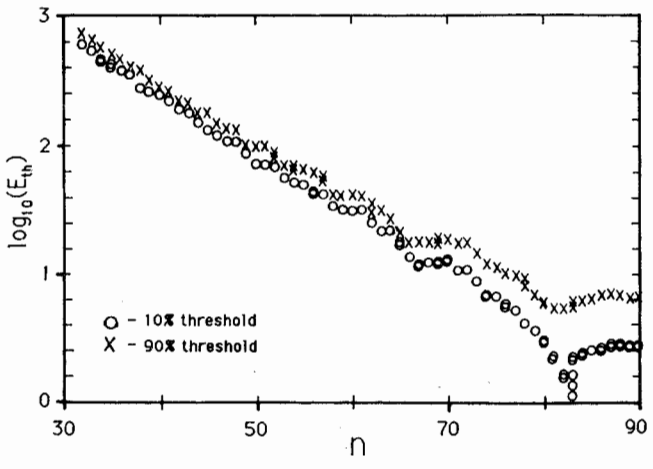

FIG. 1. Plot of the 10% (circles) and 90% (crosses) ionization thresholds initial energy level for hydrogen. The vertical axis gives the microwave peak field strength at which the given percentage of the atoms in the beam ionizes. The microwave frequency is 1.509×10^{-6} ($\nu=9.923$ GHz). (Data from Ref. [8].)

various levels of microwave field strength. These simulations show that the resonance zones corresponding to each stable region grow with the strength of the field, reaching maximum widths before they break down and join the chaotic sea. These maximum widths are close to the widths of the stable regions observed in the laboratory.

(2) The excited states of hydrogen are in the quasiclassical regime; they are on the boundary of the correspondence principle and have behavior which may be described by either Hamilton's or Schrödinger's equations. The stability can be explained in classical mechanics in terms of resonance zones, but what is the corresponding explanation in quantum mechanics? This second question is partially answered here, by showing that the hydrogen atom Hilbert space has a primary resonance structure similar to the primary resonance structure in the classical phase space. We shall also show that it may be very difficult in practice to generate the fractional resonances correctly starting from the Schrödinger equation.

The paper has three major sections. In Sec. II, we describe in some detail the resonance structure of classical microwave-driven one-dimensional hydrogen in the action-angle space of unperturbed one-dimensional hydrogen. It is in this coordinate frame that we can isolate individual primary resonances and obtain resonance conditions which allow a connection to experiment. It is also in this frame that one might hope to obtain analytic expressions for fractional resonances, and that the connection to quantum mechanics is most easily made. In Sec. III, we use the full HSH model of hydrogen to obtain strobe plots and estimates of widths of fractional resonance zones in hydrogen, and we compare our results with experiment. In Sec. IV, we use an approximation to the full Schrödinger equation for one-dimensional microwave-driven hydrogen to generate the primary resonance zones in the Hilbert space of unperturbed hydrogen. We show that the widths and positions of the quantum primary nonlinear-resonance zones are in good agreement with those obtained from classical dynamics. We also discuss why it may be very difficult, in practice to obtain an accurate picture of the fractional quantum nonlinear-resonance zones, starting from the Schrödinger equation, although this is a very important thing to do from the point of view of quantum dynamics. Finally, in Sec. V, we make some concluding remarks.

II. THE RESONANCE PICTURE

In order to obtain a clear picture of the resonance structure of microwave-driven hydrogen, we write the Hamiltonian, Eq. (1.1), in terms of action and angle variables, (I,θ), for unperturbed hydrogen. We obtain [14]

$$H=\frac{-1}{2I^2}+\frac{FI^2}{2}\sum_{M=-\infty}^{\infty}A_M\cos(M\theta-\omega t)\ , \tag{2.1}$$

where $A_0=-3$ and $A_M=2J'_M(M)/M$ for $M\neq 0$. $J'_M(z)$ is the first derivative of the Bessell function of the first kind, taken with respect to z. The values of A_M for $M\in\{1,2,\ldots,5\}$ are 0.650, 0.224, 0.118, 0.074, and 0.052.

When viewed in terms of action-angle coordinates, the HSH Hamiltonian takes the form of an infinite superposition of rotating cosine potentials, indexed by the integers, M, including a zeroth-order ($M=0$) standing cosine potential. The Mth cosine potential has amplitude $FI^2A_M/2$ and rotates through angle θ (except for $M=0$) with angular frequency ω/M. This frequency is either positive or negative (meaning an either counterclockwise or clockwise sense of rotation), according to the relative sign of M and ω. These rotating potentials can resonate with the underlying motion of the atom, which has angular frequency $d\theta/dt=1/I^3$. The resonance condition is $\omega/M=1/I^3$ or $I^3\omega\approx M$. The value $I=(M/\omega)^{1/3}$ locates the position of the Mth primary resonance in action.

If the microwave field is so weak that resonance zones do not overlap, then the motion in the neighborhood of a given resonance zone is determined largely by the cosine wave in the Hamiltonian that gives rise to that resonance. For example, in the neighborhood of the Mth primary resonance, the effective Hamiltonian is

$$H_1^{(M)}=-\frac{1}{2I^2}+\frac{FI^2A_M}{2}\cos(M\theta-\omega t)\ . \tag{2.2}$$

Thus, $H_1^{(M)}$ is a Hamiltonian which describes fairly well the qualitative behavior of the immediate neighborhood

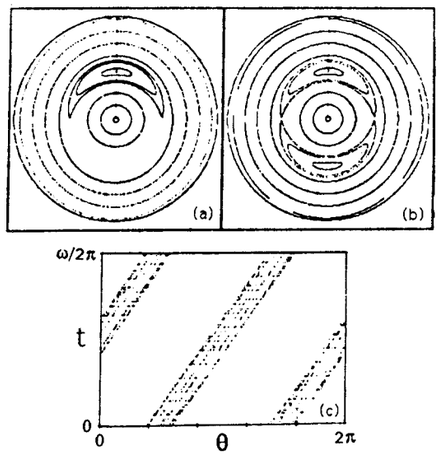

FIG. 2. Three views of the second primary HSH resonance zone, made by plotting the behavior of the singly resonant HSH system with $M=2$ in three different spaces: (a) phase paths in a frame of reference that is rotating with the cosine potential, i.e., with angular frequency ω/M (the radial coordinate is I, the angle coordinate is θ); (b) a Poincaré surface of section, made by strobing the motion at the frequency of the perturbation, ω (the radial coordinate is I, the angle coordinate is θ); (c) θ vs t for a single orbit with θ taken mod(2π) and t taken mod$(2\pi/\omega)$. The experimental parameters for all three plots are $F=2\times10^{-10}$ (1.0 V/cm) and $\omega=2\pi/(5\times10^6)$. In (a) and (b), the range of the radial coordinate, the action, is $I\in(78,162)$.

TABLE I. Locations and widths of some primary resonances for $F=2\times10^{-10}$, $\omega=2\pi/(5\times10^6)$ (classical theory and classical simulations).

	Location I_M		Width $2\Delta_M^{\text{res}}I$	
M	Theoretical $(M/\omega)^{1/3}$	Measured	Theoretical $(4M/\omega)\sqrt{FA_M/6}$	Measured
1	92.7	92.6	14.8	15.0
2	117	116	17.4	18.4
12	212	213	24.4	25.0

of the Mth primary resonance zone.

Three ways of viewing the motion of the singly resonant system [whose motion is determined by Eq. (2.2)] are shown in Fig. 2 for the case $M=2$. The *second primary resonance zone* is clearly visible in these plots. We can obtain a simple theoretical estimate of the width of those resonances by making the "pendulum approximation." This is done by expanding the energy, $-1/I^2$, about the center of the resonance, $I_M=(M/\omega)^{1/3}$, keeping terms to second order in deviations from the center, and by letting $I\to I_M$ in the coefficient of the cosine term. This gives a pendulumlike Hamiltonian. The width in action of the region enclosed by the separatrix is $(4M/\omega)\sqrt{FA_M/6}$. Table I compares the theoretical prediction of the locations and widths of selected primary resonance zones with the corresponding quantities measured in strobe plots like the one in Fig. 2(b). The primary resonance zones in HSH hydrogen are very similar in structure to the region inside the separatrix of a pendulum. If one writes the cosine term in the form $\cos(s\theta-r\omega t)$ (in this case $s=2$ and $r=1$), the plot in Fig. 2(c) provides a means of measuring the fraction s/r. An orbit satisfying the resonance condition will hit the θ axis s times and the t axis r times.

If two adjacent cosine terms are retained in the Hamiltonian Eq. (2.1), then the resulting doubly resonant system has Hamiltonian

$$H_2^{(M)}=-\frac{1}{2I^2}+\frac{FI^2}{2}\{A_M\cos(M\theta-\omega t)+A_{M+1}\cos[(M+1)\theta-\omega t]\}\ . \tag{2.3}$$

Equation (2.3) governs the behavior of the HSH system in a region of phase space between and inside the Mth and $(M+1)$th primary resonances.

A system whose Hamiltonian contains two or more cosine waves, as is the case for Eqs. (2.1) and (2.3), is nonintegrable and its phase space will contain not only the primary resonances, but an infinite hierarchy of fractional resonances. In Fig. 3, we show a strobe plot of some of the higher-order resonances lying between the primaries, $M=1$ and $M=2$, using the Hamiltonian in Eq. (2.3). The mechanism for the destruction of any KAM tori lying between these two primaries is very complex because it involves simultaneous overlap of an infinite number of these higher-order resonances. Escande and Doveil [15,16] have developed a technique for generating the Hamiltonians for these higher-order fractional resonances, and using this technique they have developed a renormalization theory to predict the destruction of any KAM torus between any pair of primaries. In the language of Escande and Doveil, each pair of primaries generates an infinite family of fractional daughter resonances. In the limit $F\to0$, these higher-order fractional resonances obey a resonance condition, $I^3\omega=s/r$, where s and r are relatively prime integers. The position in the action coordinate of a fractional resonance is given by the equation $I^3\omega=(s/r)^{1/3}$ (for $F\to0$).

We have searched the region of action I below the first primary resonance [the region $I<(1/\omega)^{1/3}$] for higher-order or fractional resonances, using Eq. (2.3) for $M=1$. In this region we expect to find fractional resonances satisfying the condition $I^3\omega=s/r<1$. The fractional resonances found there were extremely small, with widths on the order of 10^{-5}. Thus, when we use only the two-resonance approximation, the fractional resonances are not large enough to explain the plateaus in the data, even though the primaries represent the data very well. As we shall show, it takes the full series of primary resonances, which are all present implicitly in Hamiltonian Eq. (1.1), to bring the resonances in the lower region up to their full width. This is an important point when making the connection to quantum mechanics, and in trying to compute the positions and sizes of the fractional resonances theoretically.

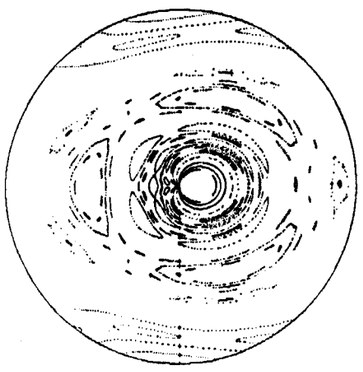

FIG. 3. Strobe plot of the doubly resonant system, Eq. (2.3), for $M=1$, $F=2\times10^{-10}$, and $\omega=2\pi/(5\times10^6)$. The radial axis is I with $95\le I\le115$ and the angular axis is θ. Several secondary and higher-order resonances are visible.

III. PHYSICAL PHASE SPACE

In classical dynamics it is possible to solve Hamilton's equations obtained from Eq. (1.1) numerically thereby including the effect of all the resonances. The appropriate phase space is the four-dimensional extended phase space $(p,x,-E,t)$, where E is the total energy of the perturbed system and t is the time. Because the Hamiltonian is periodic with period, $2\pi/\omega$, the time in the extended phase space is taken modulus $2\pi/\omega$. The extended phase space will contain periodic, quasiperiodic, and chaotic orbits. Each periodic and quasiperiodic orbit will lie on a torus. If the ratio of the frequencies of the microwave field and the atomic motion is irrational (if $I^3\omega=\alpha$, α irrational), then the trajectory is quasiperiodic and covers the torus after a long time, as is shown in Fig. 4. If the ratio of frequencies is rational ($I^3\omega=s/r$), then the trajectory is periodic and lies on the torus but does not cover it, as is shown in Fig. 5.

The most useful way of viewing the type of motion occurring in the phase space is to take a two-dimensional slice of the phase space, known as a Poincaré surface of section. The Poincaré section is a plot of p vs x at each period of the external field. A Poincaré section for the system described by Eq. (1.1) is shown in Fig. 6. The solid curves in Fig. 6 are located in resonance zones. In addition to the solid curves, there are also two orbits whose evolution is chaotic and whose Poincaré sections consist of random scatterings of dots.

In order to determine the effect of the perturbation strength on the resonance behavior, the same series of Poincaré sections as in Fig. 6 was obtained for three higher values of the microwave peak field strength, F. One of the results is shown in Fig. 7. From the analysis of a series of Poincaré sections including Figs. 6 and 7 as well as several others not shown here (cf. Ref. [17] for addition plots), the following general statements can be made about the effect of changing the perturbation strength: (1) The resonance islands grow wider with increasing perturbation strength; (2) the lower-order resonances (those for which s and r are smaller) grow faster than those of the higher-order ones; and (3) as the resonance zones grow, more and more of them decay into the "chaotic sea."

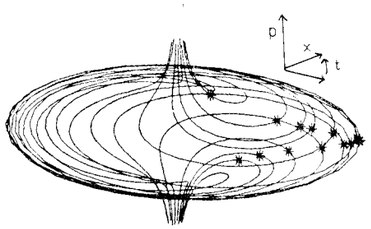

FIG. 4. A torus in the HSH model of hydrogen. The long axis is p, the radial axis is x, and the azimuthal axis is $t(\mathrm{mod}(2\pi/\omega))$. The sense of motion is down at the top, spiraling around counterclockwise, and out through the bottom. The asterisks are strobe points, and form a Poincaré section of the orbit.

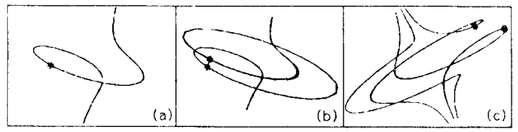

FIG. 5. Three periodic orbits (where the ratio of frequencies is a rational number): (a) $I^3\omega=1$; (b) $I^3\omega=2$; (c) $I^3\omega=\frac{2}{3}$. The asterisks are strobe points.

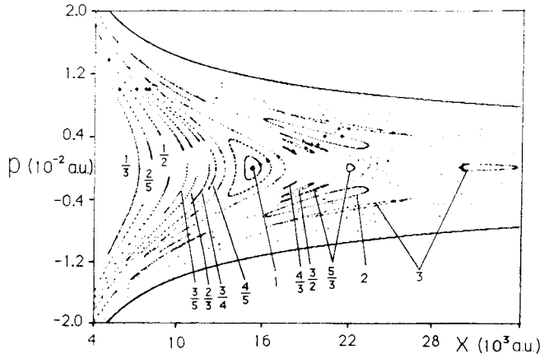

FIG. 6. Poincaré surface section (strobe plot) of HSH phase paths for various initial conditions. The perturbing electromagnetic wave has peak field strength $F=1.947\times10^{-10}$ (1.000 V/cm) and angular frequency $\omega=1.509\times10^{-6}$. The fractions labeling each island chain indicate the fraction, s/r, for that resonance zone. The outer curve is the ionization boundary (orbit for unperturbed energy $E_0=0$).

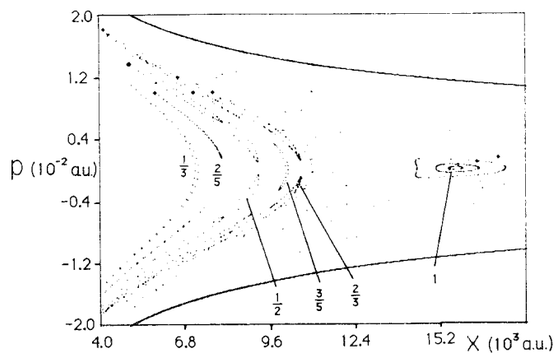

FIG. 7. Strobe plot of HSH phase paths for various initial conditions, with $F=1.095\times10^{-9}$ (5.623 V/cm) and $\omega=1.509\times10^{-6}$. This plot is equivalent to Fig. 6, except for the increased perturbation strength and an expanded scale on the x axis.

TABLE II. Experimentally and numerically measured widths of HSH resonances.

Field F	Center n	Corresponding winding number $n^3\omega$	Corresponding winding number Closest s/r	Width Lab: 10%	Width Lab: 90%	Width Simulations
0.62×10^{-8}	$59\frac{1}{2}$ or 60	0.32	$\frac{1}{3}$ (0.33)	3 or 4	4	4.0
1.90×10^{-9}	$62\frac{1}{2}$	0.37	$\frac{3}{8}$ (0.38)	0	2	<0.1
1.90×10^{-9}	$63\frac{1}{2}$	0.39	$\frac{2}{5}$ (0.40)	2	0	0.1
1.90×10^{-9}	$68\frac{1}{2}$ or 69	0.49	$\frac{1}{2}$ (0.50)	4	5 or 7	8.9
1.90×10^{-9}	$71\frac{1}{2}$	0.55	$\frac{4}{7}$ (0.57)	2	0 or 2	<0.1
1.90×10^{-9}	$74\frac{1}{2}$	0.62	$\frac{3}{5}$ (0.60)	2	0 or 2	0.7
1.10×10^{-9}	$76\frac{1}{2}$	0.68	$\frac{2}{3}$ (0.67)	0 or 2	2	1.8
1.90×10^{-10}	87 or 88	1.01	$\frac{1}{1}$ (1.00)	>8	>10	11.9

Table II compares these data with the experimental results shown in Fig. 1. The left-hand column gives the microwave field strength. The second column from the left locates the center of the regions of suppressed ionization, or enhanced stability, in the laboratory data. The next two columns show how closely these centers match the low-order rational winding numbers. Finally, the last three columns compare the widths of these regions with the *largest* width reached by the corresponding resonance zones before decaying into the chaotic sea. (In the Appendix we explain how these widths are obtained.) Columns 2–4 confirm what has been noted by Jensen [13], namely, that the locations of the regions of stability are well predicted by the locations of fractional resonance zones in the phase space. However, no one has previously offered an explanation of the widths of these regions, or a correspondence between the widths in the laboratory and numerical data as is done in the last three columns of the Table II. (Some fractional resonances have also been observed by Leopold and Richards [18].)

The laboratory and numerical data are in qualitative agreement on the widths of the various resonance zones. The zones may be listed by winding number in order of decreasing width: $s/r=1,\ \frac{1}{2},\ \frac{1}{3},\ \frac{2}{3},\ldots$. The significance of this ordering is that the width of the zones decreases as the sizes of the integers in the numerator and denominator of the winding numbers increases. Some additional data on the growth of fractional resonances with increasing field strength is given in Table III.

In conclusion, the widths of the regions of suppressed ionization in Fig. 1 are well correlated with the widths of the corresponding HSH resonance zones. The zones expand with increasing perturbation strength, and each resonance zone reaches a maximum width before decaying into the chaotic sea. The widths of the regions of supressed ionization are on the order of these maximum widths achieved by the resonance zones.

IV. QUANTUM DYNAMICS

The bound-state energy eigenvalues (in atomic units) of the unperturbed hydrogen atom are given by

TABLE III. Locations and extents in action of resonance islands for $\omega=1.5\times10^{-6}$ and various field strengths. (The $s/r=1$ resonance shrinks in overall size with increasing F as its outer layers decay into chaos, but as F increases it becomes very elongated causing an overall increase in "width.")

	Measured action (average, width, excursion)			
s/r	$F=1.9\times10^{-10}$	$F=1.1\times10^{-9}$	$F=1.9\times10^{-9}$	$F=0.62\times10^{-8}$
$\frac{1}{3}$	60.3, 0.0, 0.2	60.4, 0.3, 1.4	60.7, 0.6, 3.0	60.7, 4.0, 11.1
$\frac{2}{5}$	64.1, 0.0, 0.3	64.1, 0.0, 1.6	63.6, 0.1, 1.0	
$\frac{1}{2}$	69.1, 0.6, 1.1	69.6, 4.0, 6.3	70.0, 8.9, 14.2	
$\frac{3}{5}$	73.5, 0.1, 1.1	73.6, 0.3, 6.1	73.6, 0.7, 9.8	
$\frac{2}{3}$	76.0, 0.1, 1.2	76.3, 1.8, 8.1		
$\frac{3}{4}$	79.2, 0.1, 2.3	78.9, 1.0, 10.7	chaotic	
$\frac{4}{5}$	80.9, 0.1, 2.9	chaotic		
1	87.4, 11.9, 11.9	88.7, 8.2, 8.2	89.9, 11.1, 11.1	
$\frac{4}{3}$	95.9, 0.8, 2.5			
$\frac{3}{2}$	100.1, 1.9, 2.8			
$\frac{5}{3}$	103.4, 2.3, 4.3		chaotic	
2	110.1, 8.4, 8.4			
3	126.0, 8.0, 8.1			

$E_n = -1/2n^2$, where n is the principal quantum number. The energy-level spacing is given by the Balmer formula

$$E_{n+1} - E_n = \frac{1}{2}\left[\frac{1}{n^2} - \frac{1}{(n+1)^2}\right] \xrightarrow[n\to\infty]{} \frac{1}{n^3}, \quad (4.1)$$

which, for large values of the principal quantum number, approaches the same form as the frequency of the orbital motion in classical action-angle coordinates, with $I \to n$.

The contribution to the HSH Hamiltonian matrix which couples extreme Stark bound states to one another can be written

$$H_{n',n} = -\frac{1}{2n^2}\delta_{n',n} + F\langle n'|\hat{x}|n\rangle\cos(\omega t), \quad (4.2)$$

where $|n\rangle = |n;0,n+1,0\rangle$. If we retain only matrix elements of the form Eq. (4.2) in the Hamiltonian matrix we can then study the resonance structure along the extreme Stark ladder. For $n > 30$, the coupling to other bound states will be small [19]. If we wish to focus on the region of Hilbert space influenced by the lower primaries (in the experiments we consider here this is the regime $30 < n$), we can truncate the Hamiltonian further and write

$$\hat{H}|n\rangle \approx -\frac{1}{2n^2}|n\rangle + \frac{Fn^2}{4}\sum_{M\gg -n}^{\ll n} A_M(e^{i\omega t}|n+M\rangle + e^{-i\omega t}|n-M\rangle). \quad (4.3)$$

To obtain Eq. (4.3), we have expanded $\cos(\omega t)$ in exponentials and we have relabeled summation variables. As long as the energy of the atom in the presence of the microwave cannot diffuse below $n = 30$, and as long as the resonances have not overlapped, so that there is no ionization, then Eq. (4.3) gives a good approximation to the behavior of HSH for $30 < n$. Note that we have used the fact that $\langle n+M|\hat{x}|n\rangle \approx n^2 A_M/2$ for the values of n and M we are considering (we have checked that it gives values to within 1% of the fully quantum values). In Eq. (4.3), we have rewritten Eq. (4.2) in a form which explicitly shows its resonance structure (cf. Refs. [20–22] for an extensive discussion concerning the structure of quantum nonlinear resonances).

In classical action-angle coordinates, resonance can occur between the frequency of rotation of the unperturbed system and the frequency of rotation of a set of cosine potentials. In the quantum system, the microwave perturbation is in resonance with the atom if its photon size is a multiple, by some M, of the level spacing of the atom (this gives the primary resonances). So the resonance condition is, for large n, $n^3\omega \approx M$, where $|M| \ll n$. This is identical to the primary resonance condition in the classical case.

The Hamiltonian in Eq. (4.3) can be used in Schrödinger's equation and Schrödinger's equation can be solved numerically. The resulting simulations demonstrate a phenomenon very similar to the classical resonance behavior in that there are regions of confinement of probability in the space of energy levels. Furthermore, these regions expand and merge as F is increased, as do the resonance zones in the classical theory.

The entire time evolution of an atom, starting with the turn-on of the perturbation, may be presented in a single, static picture by using shading to represent the magnitude of probability. The result is called here an *evolution plot,* and is shown in Fig. 8. Any vertical slice through this figure contains the same information as a probability plot at a single time. This technique makes it possible to see many aspects of the motion that are not evident from inspecting series of individual frames. In Fig. 8, the probability spreads out evenly both above and below the initial state. After spreading out to fill the region from about $n = 69$ to 95, the probability stays in this region, yet with some oscillation in its structure. The region through which the probability has spread is identified as the first primary resonance zone.

A further compaction of the data brings out evidence of the resonance zones even more clearly. In Fig. 8, the essential features of the probability distribution remain fairly stable after the initial spreading occurs although oscillation of probability does occur with time. This suggests that the essential information about a single evolution is preserved if the entire plot is collapsed by averaging the probabilities, for each energy eigenvalue, over time, starting from the time when the maximum width is first reached. This reduces each evolution plot to a vertical slice so that a series can be juxtaposed to form a type of plot which we call a *distribution plot.* The distribution plot, obtained from a series of evolution plots for the first primary resonance ($M = 1$), is shown in Fig. 9. Both the vertical and horizontal axes are measured in the index of the principal quantum number. A value on the horizontal axis denotes the initial condition of one particular calculation. A value on the vertical axis denotes a possible state in the energy-index space of each calculation. The shade of the plot at the intersection of these two values indicates the extent to which probability has spread from the initial energy state, n_0, to a state with principal quantum number indicated on the vertical axis. In the distribution plot, the resonance zone shows up as a distinctive square pattern. The probability spreads out to fill the square area in a manner which is almost completely independent of the initial state of the atom. This plot is a compact representation of a large amount of data. It

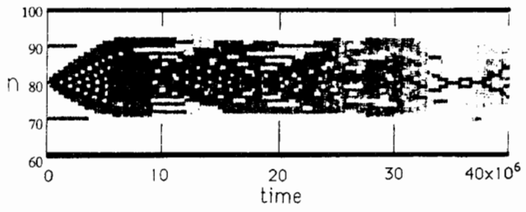

FIG. 8. Evolution plot for the singly resonant HSH system in quantum mechanics with $M = 1$ and $n_0 = 80$. The probability is seen to spread within a specific range of energy levels, and not beyond. This is the first primary resonance zone in the quantum system. The experimental parameters are $F = 0.95 \times 10^{-9}$ (4.9 V/cm) and $\omega = 80^{-3} = 1.9 \times 10^{-6}$.

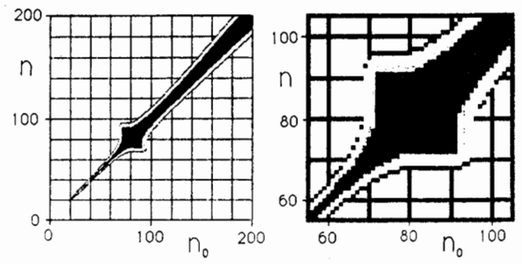

FIG. 9. Distribution plot for the singly resonant HSH atom with $M = 1$. The plot on the left shows the series of initial states from $n_0 = 20$ to 200. The plot on the right is an expanded view of the vicinity of the resonance zone. The experimental parameters are the same as in Fig. 9.

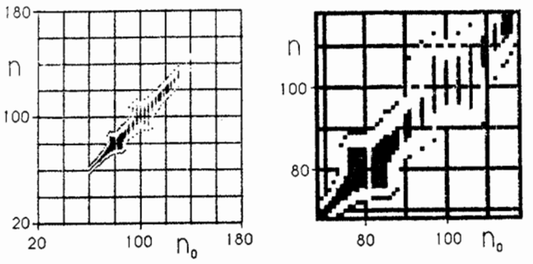

FIG. 10. Distribution plots for the doubly resonant case with $M \in \{1,2\}$, $F = 1.9 \times 10^{-10}$ (0.98 V/cm) and $\omega = 80^{-3} = 1.9 \times 10^{-6}$. The first and second primary resonance zones are visible.

comprises vertical slices for time series for each of 181 initial states, with the probabilities in each slice being obtained by averaging over several hundred, and in many cases upwards of a thousand, time frames.

Table IV compares the classical theoretical estimates (with $I \to n$) of the locations and widths of the resonances with the values measured from the evolution and distribution plots. The results of the simulations are seen to be in good agreement with the predictions, although the resonance zones seem to be somewhat narrower than predicted. While most of the experimental work on excited states of hydrogen has investigated ionization, there are a few results reported [4] that relate directly to the simulations presented in this section. These are measurements of the final-state distribution for a beam initially prepared in a particular excited state, and perturbed in a microwave chamber. Unfortunately, none of these data have been taken with a set of parameters that would test for primary resonance zones.

Figures 10 and 11 show distribution plots for Eq. (4.3) with $M \in \{1,2\}$. The microwave frequency is the same as is used in Fig. 9, but the field strength is reduced by a factor of 5. The first and second primary resonance zones are clearly visible. The energy of an atom in the region of one of these zones spreads in probability through that zone and does not enter the other zones. In Fig. 11, the parameters F and ω are the same as Fig. 9. The calculations for the doubly resonant system require much more computer time than for the singly resonant. This is the reason for the gaps in the data seen in Figs. 10 and 11. Despite the gaps due to high computation costs, this plot shows a definite overlap of the resonance regions. The square area extends from about 70 to 120, the energy indices of which correspond to the lower edge of the first primary resonance zone and the upper edge of the second. For an initial state in either resonance zone, the probability spreads throughout both zones. In most parts, the probability still stays primarily in the original zone, with only very little spreading into the other zone. For $n_0 = 90$, however, which is midway between the locations of the two zones, the probability is fairly evenly spread out. This is the quantum analog of resonance overlap.

Approximations of the type used to obtain Eq. (4.3) do not contain enough information to accurately generate the fractional resonances in hydrogen, although Eq. (4.3) does reproduce the primary resonances quite well. Quantum fractional resonances have been observed in other quantum systems [21,22]. A remaining problem in the theory of microwave-driven hydrogen is to find a theoretical treatment that will allow us to see them numerically.

V. CONCLUSIONS

In both classical and quantum mechanics, harmonically driven Stark states of hydrogen (HSH) exhibit nonlinear resonance between the orbital motion of the atom and the microwave perturbation. In classical mechanics,

TABLE IV. Locations and widths of some primary resonances for $F = 0.95 \times 10^{-9}$, $\omega = 80^{-3}$ (classical theory and quantum-mechanical simulations).

	Location n_M		Width $2\Delta_M^{res} n$	
M	Theoretical $(M/\omega)^{1/3}$	Measured	Theoretical $(4M/\omega)\sqrt{FA_M/6}$	Measured
1	80	80	21	16
2	101	101	24	20
3	115	116	27	22
4	127	126	28	26
5	137	135	29	28

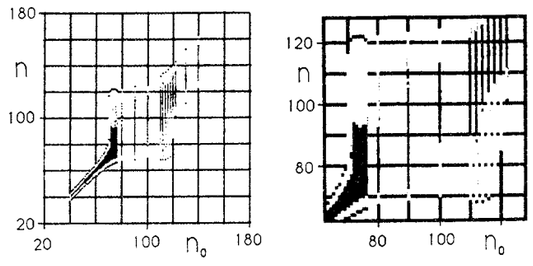

FIG. 11. Distribution plots for the doubly resonant HSH atom with $M \in \{1,2\}$, $F = 0.95 \times 10^{-9}$ (4.9 V/cm), and $\omega = 1.9 \times 10^{-6}$. The first and second primary resonance zones have gone through overlap.

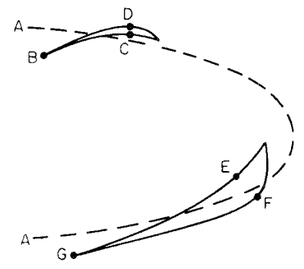

FIG. 12. The two different measures of extent in action of a chain of resonance islands. The dotted line A is the line of constant action for the average value of the action in the chain. The pairs of points $\{C,D\}$ and $\{E,F\}$ appear opposite each other at the widest parts of the two islands. The point G has the largest value of action for this chain, the point B the smallest. The *width* of the chain is the largest width of all of its islands, i.e., $I_F - I_E$ for this example. The *excursion* is the difference between the largest and smallest values of action in all of its islands, i.e., $I_G - I_B$ here. The combination of shapes shown here is an atypical exaggeration of the shape of an island chain, in order to express the meaning of *width* and *excursion*.

the primary resonances occur when the angular frequency, in action-angle space, of the unperturbed atom is close to the frequency of one or more of an infinite number of rotating cosine potentials representing the perturbation. In quantum mechanics, the primary resonances arise when the energy-level spacing of the unperturbed atom is close to an integer multiple of the microwave photon size.

These results demonstrate that, despite totally different mathematical foundations, both classical and quantum mechanics do demonstrate the existence and overlap of resonance zones. Moreover, the locations and sizes of these zones are the same in both theories. In classical mechanics these are zones in the atom's phase space, and may be plotted in either the physical or action-angle coordinates. In quantum mechanics they are zones in the space of the atom's energy levels, which correspond to subspaces in its Hilbert space.

In classical mechanics, the growth of the fractional resonance zones has been shown here to explain the widths of the regions of suppressed ionization in the experiments done by Koch. While others have explained the locations of these regions in terms of resonance zones, we show that their widths are explained also by this same theory.

The conclusions of this work may be summed up as follows: (1) The HSH atom demonstrates nonlinear resonance by the existence and overlap of resonance zones in both a classical and quantum analysis; (2) simulations based on the classical equations of motion reproduce the detailed behavior observed in the laboratory. Specifically, the positions and widths of regions of stability calculated in the physical phase space match those found in the laboratory; (3) simulations based on the quantum equations of motion agree with the spreading of states observed in the laboratory, and with the size and overlap of primary resonance zones calculated in the classical action-angle coordinates. Perhaps one of the most important results is that it is not possible to reproduce, accurately, the fractional resonances $s/r < 1$ by using approximations to the HSH system which retain only a few of the primary resonances.

ACKNOWLEDGMENT

The authors wish to thank the Welch Foundation of Texas, Grant No. F-1051, for partial support of this work.

APPENDIX

There are two different measures of the extent, in action, of an island chain. These measures are illustrated in Fig. 12. The *width* of an individual island is the largest difference in action value of *points appearing opposite each other* on the island. The width of a chain of islands is the largest width of all of its islands. The *excursion* of an island chain is the overall difference in action encountered in traversing the whole chain.

The correct value of both the width and the excursion are obtained from measuring the outermost set of closed curves among the concentric curves forming the island (the *separatrix).* In compiling the data for Table II, it was always the objective to generate an island chain as close to the separatrix as possible for measurement.

*Permanent address: Ennex Technology Marketing, Inc., 825 W. 11th Street, Suite One, Austin, TX 78701.

[1] J. E. Bayfield and P. M. Koch, Phys. Rev. Lett. **33**, 258 (1974).

[2] J. E. Bayfield and L. A. Pinnaduwage, J. Phys. B **18**, L49 (1984).

[3] J. E. Bayfield and L. A. Pinnaduwage, Phys. Rev. Lett. **56**, 1007 (1985).

[4] J. N. Bardsley, B. Sundaram, L. A. Pinnaduwage, and J. E. Bayfield, Phys. Rev. Lett. **56**, 1007 (1985).

[5] K. A. H. van Leeuwen, G. V. Oppen, S. Renwick, J. B. Bowlin, P. M. Koch, R. V. Jensen, O. Rath, D. Richards, and J. G. Leopold, Phys. Rev. Lett. **55**, 2231 (1985).

[6] P. M. Koch, K. A. H. van Leeuwen, O. Rath, D. Richards, and R. V. Jensen, in *The Physics of Phase Space,* edited by H. Araki, J. Ehlers, K. Hepp, R. Kippenhahn, H. A. Widenmuller, J. Wess, and J. Zittartz (Springer-Verlag, Berlin, 1987).

[7] M. M. Sanders, R. V. Jensen, P. M. Koch, and K. A. H. van Leeuwen, Nucl. Phys. B **2**, 578 (1987).

[8] P. M. Koch, in *Electronic and Atomic Collisions,* edited by H. B. Gilbody, W. R. Newell, F. H. Read, and A. C. H. Smith (North-Holland, Amsterdam, 1988).

[9] J. E. Bayfield and D. W. Sokol, Phys. Rev. Lett. **61**, 2007 (1988).

[10] E. J. Galvez, B. E. Sauer, L. Moorman, P. M. Koch, and D. Richards, Phys. Rev. Lett. **61**, 2011 (1988).

[11] J. E. Bayfield, G. Casati, I. Guarneri, and D. W. Sokol, Phys. Rev. Lett. **63**, 364 (1989).

[12] L. D. Landau and E. M. Lifshitz, *Quantum Mechanics* (Pergamon, Oxford, 1977), Sec. 37.

[13] R. V. Jensen, Phys. Scr. **35**, 668 (1986).

[14] R. V. Jensen, Phys. Rev. A **30**, 386 (1983).

[15] D. F. Escande and F. Doveil, J. Stat. Phys. **26**, 257 (1981).

[16] D. F. Escande, Phys. Scr. **T2/1**, 126 (1982).

[17] Marshall Burns, Ph.D. dissertation, University of Texas at Austin, 1991.

[18] J. G. Leopold and D. Richards, J. Phys. B **19**, 1125 (1985).

[19] J. N. Bardsley and B. Sundaram, Phys. Rev. A **32**, 689 (1985).

[20] L. E. Reichl and W. A. Lin, Phys. Rev. A **33**, 3598 (1986).

[21] L. E. Reichl, Phys. Rev. A **39**, 4817 (1989).

[22] L. E. Reichl and Li Haoming, Phys. Rev. A **42**, 4543 (1990).